Magnetic ordering in $PrBa_2Cu_{3-y}Al_yO_{6+x}$

A. Longmore, A. T. Boothroyd, Chen Changkang, and Hu Yongle
Clarendon Laboratory, Oxford OX1 3PU, England

M. P. Nutley*
Institut Laue-Langevin, 38042 Grenoble Cedex, France

N. H. Andersen, H. Casalta, and P. Schleger
Department of Solid State Physics, Risø National Laboratory, DK-4000 Roskilde, Denmark

A. N. Christensen
Institute of Chemistry, University of Århus, DK-8000 Århus, Denmark

(Received 14 July 1995)

The magnetic ordering in single crystals of $PrBa_2Cu_3O_{6+x}$ has been investigated by elastic neutron scattering over the full range of temperatures for reduced and oxygenated crystals. The crystals were grown in alumina crucibles and therefore contained dissolved aluminum on the Cu(1) site. Both aluminum and oxygen contents were analyzed in detail in order to establish their effects on the magnetic ordering. Our crystals exhibited Pr ordering and the two types of antiferromagnetic Cu ordering frequently reported in related compounds, but our results differ in several respects from previous studies. We observed three-dimensional (3D) collinear ordering of the Pr moments in the oxygenated crystal, with a finite correlation length of (34 ± 3) Å parallel to the *c* axis, but in contrast to earlier neutron scattering results, which tentatively placed the Pr moment as being parallel to the *c* axis, we find the moment to be aligned well away from the *c* axis, in agreement with recent $^{170}Yb^{3+}$ Mössbauer spectroscopy results. Ridges of scattering indicative of 2D magnetic ordering were seen in both oxygenated and reduced crystals, though we believe different magnetic moments are responsible in each case. The Pr Néel temperatures were suppressed compared with those reported for nominally pure samples. We have observed a very small 3D-ordered moment on the Cu(1) site in the second type of Cu antiferromagnetic ordering (in the reduced crystal), but an ordered Cu(1) moment may not necessarily be a characteristic of this structure. Our results are discussed with reference to previous works, and in the light of the Al substitution.

I. INTRODUCTION

The suppression of superconductivity by praseodymium in a number of families of cuprate superconductors, particularly in $PrBa_2Cu_3O_7$,[1] is an outstanding issue in the field of high-T_c superconductivity. A successful explanation of the suppression effect will require a detailed understanding of the hole-doped CuO_2 layers and of the superconductivity frequently associated with them. For this reason, studies of the nonsuperconducting, Pr-containing cuprates may help us to understand superconducting materials.

Experiments that are directly sensitive to the valence of Pr in $PrBa_2Cu_3O_{6+x}$ have provided overwhelming evidence for a 3+ valence state,[2] though the Pr $4f$ orbitals almost certainly hybridize with O $2p$ states on the CuO_2 planes. Such a Pr-CuO_2 coupling may be responsible for the anomalously high magnetic ordering temperature of the Pr sublattice.[3–5] A comparison of $YBa_2Cu_3O_7$ and $PrBa_2Cu_3O_7$ by electron-energy-loss spectroscopy[6] (EELS) was taken to indicate that the hole density on the CuO_2 planes is not significantly affected by Pr substitution, which is evidence for a straight substitution of Pr^{3+} for Y^{3+}. On the other hand, the occurrence of long-range antiferromagnetic order of the Cu moments on the planes in $PrBa_2Cu_3O_7$ is rather surprising because such antiferromagnetism is characteristic of *undoped* CuO_2 planes, as observed in $YBa_2Cu_3O_{6+x}$ (i.e., the holes in $PrBa_2Cu_3O_7$ resulting from the 3+ valence of Pr have not disrupted the magnetic ordering of the CuO_2 planes). Furthermore, if there are holes on the planes in $PrBa_2Cu_3O_7$, then why do they not superconduct like in $YBa_2Cu_3O_7$?

Models of the superconductivity suppression based on hybridization of the Pr $4f$ electrons with the CuO_2 planes (such as that of Fehrenbacher and Rice[7]) will have implications for the magnetic couplings between the different ions and, hence, for magnetic ordering. Experimental data on the types of exchange interactions, magnetic structures, and ordering temperatures could be important to help evaluate different models for $PrBa_2Cu_3O_{6+x}$, and our neutron diffraction experiments described here are an attempt to provide such information in greater detail.

The magnetic phase diagram of $PrBa_2Cu_3O_{6+x}$ has been established by various techniques, including neutron diffraction. Mössbauer,[5] muon,[8] and nuclear magnetic resonance spectroscopy[9] revealed that the Cu(2) moments begin to order antiferromagnetically at, or slightly above, room temperature in polycrystalline samples of $PrBa_2Cu_3O_{6+x}$ and that the ordering temperature increases slightly as oxygen is removed.

Magnetic ordering of the Pr sublattice, observed in bulk measurements on polycrystalline $PrBa_2Cu_3O_7$,[3–5] occurs at

TABLE I. Structure refinement of the Oxford oxygenated crystal. $R_w(F)$ was 6.2%. The amount of oxygen present from the Cu-O chain layers is 0.913(9) per chemical unit cell, indicating near-complete oxidation, with the total oxygen content being 6.731(11). Because of the near tetragonality of the sample, it is quite difficult to distinguish between the O(1) and O(5) sites, and so the sum of their occupancies, 0.913(9), is given.

	x	y	z	Occupancy	U_{11}	U_{22}	U_{33}
Pr	0.5	0.5	0.5	0.998(8)	0.0087(8)		0.0087(10)
Ba	0.5	0.5	0.18474(15)	0.993(5)	0.0125(5)		0.0108(7)
Cu(1)	0	0	0	0.750(5)	0.028(1)		0.008(1)
Cu(2)	0	0	0.35089(9)	1	0.0068(2)		0.0111(4)
O(1)	0	0.5	0	} 0.913(9)	0.036(2)	0.019(2)	0.016(2)
O(5)	0.5	0	0		0.019(2)	0.036(2)	0.016(2)
O(2)	0.5	0	0.3702(1)	1	0.0080(3)		0.0143(6)
O(3)	0	0.5	0.3689(1)	1	0.0080(3)		0.0143(6)
O(4)	0	0	0.1537(2)	0.909(5)	0.042(1)		0.024(1)

17 K. From neutron diffraction measurements on polycrystalline samples,[4] a simple magnetic structure was proposed in which the Pr moments point along the c axis (a ''tentative'' result) and order antiferromagnetically in all three crystallographic directions. The Pr ordering temperature decreases with decreasing oxygen content,[10,11] but according to neutron powder diffraction[12] the magnetic structure appears to remain the same apart, perhaps, from a possible broadening of the peaks along the c axis, indicating a shorter correlation length in this direction.

The copper magnetic orderings described in this paper are referred to in the following way, h, k, and l being integers. ''Type I'' refers to the phase when reflections are only seen at $(h+\frac{1}{2},k+\frac{1}{2},l)$, and ''type II'' refers to the phase when reflections are seen at $(h+\frac{1}{2},k+\frac{1}{2},l+\frac{1}{2})$. ''Type-II intermediate'' means that the $(h+\frac{1}{2},k+\frac{1}{2},l)$ peaks are still present, and ''type-II ground state'' means that they are absent. This simple naming system, based on what is actually observed, avoids the potential danger of implying *a priori* any physical interpretation. In most experiments on $RBa_2Cu_3O_{6+x}$ compounds (R=lanthanide), when the copper magnetism changes it does so in the sequence *paramagnetic→type I → type-II intermediate→type-II ground state* as temperature decreases.

The direct transition *paramagnetic→type-II ground state* has also been reported on one occasion, in the only previous single-crystal neutron diffraction study of magnetic order in $PrBa_2Cu_3O_{6+x}$.[13] In that work, the magnetic ordering of the Cu moments was investigated in a crystal after different annealing treatments. Néel temperatures of at least 370 K were reported for the copper ordering, which is somewhat higher than that found with polycrystalline samples by the local probes listed above. In samples with larger values of x both type-I and type-II copper orderings were observed.

In our experiments we also observed the Cu type-I and type-II phases, as well as Pr ordering. Our results, however, differ in many respects from the single-crystal[13] and powder[4,12] neutron diffraction investigations summarized above. It is likely that different amounts of sample impurities are responsible for many of these discrepancies. For neutron diffraction a relatively large crystal (>10 mg) is required to obtain good magnetic reflections. At the time of these experiments, the only suitable crystals available were grown in alumina crucibles, and so the crystals contained dissolved Al, which has been found previously to substitute onto the Cu(1) sites.[14] Results from similar crystals are widespread in the literature and are of value as long as the impurity level is known. Our crystals of Al-doped $PrBa_2Cu_3O_{6+x}$ have been very thoroughly characterized by neutron diffraction and mass spectrometry. In this way we can establish by comparison with results from Al-free crystals (when they become available), which properties are characteristic of the pure compound and which properties are due to the presence of Al substitution. It would then be interesting to compare the latter properties with the results of other doping studies.

II. SAMPLE CHARACTERIZATION

Three single crystals were investigated, two of them grown in Oxford and one in Århus. The crystals were prepared in alumina crystals, and so a degree of Al doping onto the Cu(1) (chain-layer) site is to be expected. The method of crystal growth of the Oxford crystals has been described elsewhere.[15] One of the Oxford crystals (mass 30 mg) was annealed in nitrogen gas to remove oxygen (hereafter referred to as the ''reduced crystal''). The other crystal from Oxford (mass 100 mg) and the Århus crystal (mass 50 mg) were annealed in oxygen for 6 months (hereafter referred to as the ''oxygenated crystal'' and the ''Århus crystal''). Most of the data presented here are from the reduced and oxygenated Oxford crystals.

We established the oxygen content of the Oxford crystals by refining their structures on the neutron four-circle diffractometer TAS2 at Risø. The refined structural parameters are given in Tables I and II. The lattice parameters used for the oxygenated crystal were 3.873, 3.928, and 11.710 Å (obtained by Jorstarndt *et al.*[16] for $PrBa_2Cu_3O_7$), and those used for the reduced crystal were 3.908, 3.908, and 11.844 Å (obtained by López-Morales *et al.*[17] for $PrBa_2Cu_3O_6$). The total oxygen content of the oxygenated crystal is 6.73(1), and for the reduced crystal it is 6.40(6). These numbers, however, do not reflect the true oxygen content of the chain-layer sites, due to a significant underoccupancy of the O(4) apical oxygen site. The combined contents of the chain-layer oxygen sites [O(1),O(5)] are 0.913(9) and 0.28(3) for the oxygenated and reduced crystals, respectively. These chain-layer oxygen occupancies better reflect the effect of the different annealing treatments given to the two crystals. The depletion of the

TABLE II. Structure refinement of the reduced crystal. $R_w(F)$ was 6.0%. The amount of oxygen present in the Cu-O chain layers is 0.56(4) per chemical unit cell, with the total oxygen content being 6.40(6).

	x	y	z	Occupancy	U_{11}	U_{22}	U_{33}
Pr	0.5	0.5	0.5	1	0.0043(13)		0.0092(19)
Ba	0.5	0.5	0.1884(3)	1	0.0102(7)		
Cu(1)	0	0	0	0.80(3)	0.025(2)		0.006(2)
Cu(2)	0	0	0.3511(2)	1	0.0032(6)		0.0105(10)
O(1)/O(5)	0	0.5	0	0.28(3)	0.036(10)	0.005(6)	0.021(7)
O(2)/O(3)	0.5	0	0.3694(2)	1	0.0083(6)		
O(4)	0	0	0.1520(4)	0.92(3)	0.036(2)		0.020(2)

O(4) site in $PrBa_2Cu_3O_{6+x}$ crystals was also observed in x-ray diffraction measurements by Lowe-Ma and Vanderah.[18]

Because of the likelihood of vacancies, as well as Al and Cu, occupying the Cu(1) sites, it is not possible to determine the Al content from diffraction alone. The Cu(1) occupancies given in Tables I and II are based on zero Al content and are lower than the values given by Lowe-Ma and Vanderah. In order to establish the Al content independently, we took a small fragment (approximately 10 mg) from the Oxford oxygenated crystal and analyzed the cation ratios by inductively coupled plasma mass spectrometry (ICPMS). We also measured as a control a small crystal of Al-free $PrBa_2Cu_3O_{6+x}$ grown by Th. Wolf in Karlsruhe. Table III lists the cation ratios obtained from these samples. The Pr:Ba:Cu ratio observed for the Al-free crystal is very close to the ideal 1:2:3, but for the Oxford crystal there are noticeable deviations from the ideal stoichiometry. First, the Pr:Ba ratio is greater than 1:2, which is an indication of excess Pr on the Ba site. In fact, we know there is Pr on the Ba site because we have observed it directly on this same crystal, and also on another from a similar batch, by polarized neutron diffraction.[19] Second, the amount of Cu present is approximately 20% lower than the ideal ratio. This is partly accounted for by the observed concentration of Al, which from Table III is approximately 4% of the total amount of Cu. Measurements by electron probe microanalysis (EPMA) of other $PrBa_2Cu_3O_{6+x}$ crystals grown in Oxford have revealed Al concentrations of between 6% and 9% of the Cu.[15] Assuming that the Cu(2) sites are fully occupied by Cu, then we estimate that only 57% of the Cu(1) sites are occupied by Cu, 12% contain Al, and the remaining 31% are vacant. In summary, the chemical formula of the Oxford oxygenated crystal is $Pr(Ba_{2-z}Pr_z)Cu_{3-y-v}Al_yO_{6+x}$, with $x=0.73$, $y=0.12$, $z=0.048$, and v (vacancies)$=0.31$.

TABLE III. Cation ratios measured on (i) the Oxford oxygenated crystal and (ii) an Al-free $PrBa_2Cu_3O_{6+x}$ crystal, by Inductively-Coupled Plasma Mass Spectrometry.

Element	(i)	(ii)
Pr	0.184	0.166
Ba	0.343	0.340
Cu	0.452	0.494
Al	0.021	

III. EXPERIMENTAL DETAILS

The neutron measurements were carried out on the TAS1 triple-axis spectrometer at Risø. The (002) reflection of pyrolitic graphite was selected for the analyzer (when used) and monochromator. Neutrons of incident energy 13.7 meV were employed, and a graphite filter was placed before the sample to eliminate higher orders. The in-plane collimation was 60′-30′-sample-60′-open. For measurements below room temperature, the crystals were mounted in either a ^{4}He cryostat or a closed-cycle refrigerator, and to reach higher temperatures a furnace was used. The total range of temperatures measured was from 1.6 to 380 K. The crystals were aligned with the (1,1,0) and (0,0,1) reciprocal lattice vectors defining the scattering plane. Scans through the Bragg peaks were either linear in reciprocal space, for example parallel to $(h,h,0)$ and $(0,0,l)$, or were ω scans, depending on which was more appropriate.

IV. THEORY

The intensity of diffraction from a noncollinear magnetic structure at a scattering vector $\mathbf{K}$ is proportional to

$$I(\mathbf{K})=\sum_{\alpha,\beta}\langle(\delta_{\alpha\beta}-\hat{K}_\alpha\hat{K}_\beta)F^\alpha(\mathbf{K})F^{\beta*}(\mathbf{K})\rangle \quad (\alpha,\beta=x,y,z), \tag{1}$$

where $\langle\ \rangle$ denotes a domain average (we assume that an equal population of domains exists), $\delta_{\alpha\beta}$ is the Kronecker delta, $\hat{K}_\alpha$ is the α component of the unit scattering vector, and $F^\alpha(\mathbf{K})$ is the (vector) magnetic structure factor given by

$$F^\alpha(\mathbf{K})=\sum_j \mu_j^\alpha f_j(\mathbf{K})\exp(i\mathbf{K}\cdot\mathbf{r}_j), \tag{2}$$

where j labels the magnetic moments in the unit cell, μ_j^α is the α component of the jth moment, $f_j(\mathbf{K})$ is the form factor of that moment, and $\mathbf{r}_j$ is its position.

For the case of a collinear arrangement of magnetic moments of the same magnitude μ (i.e., all the moments are either parallel or antiparallel to a particular direction), this can be simplified:

$$\mu_j^\alpha=\sigma_j\mu^\alpha, \tag{3}$$

where $\sigma_j=\pm1$, so that

$$I(\mathbf{K})=\mu^2[1-(\hat{\mathbf{K}}\cdot\hat{\boldsymbol{\mu}})^2]\left|\sum_j \sigma_j f_j(\mathbf{K})\exp(i\mathbf{K}\cdot\mathbf{r}_j)\right|^2. \tag{4}$$

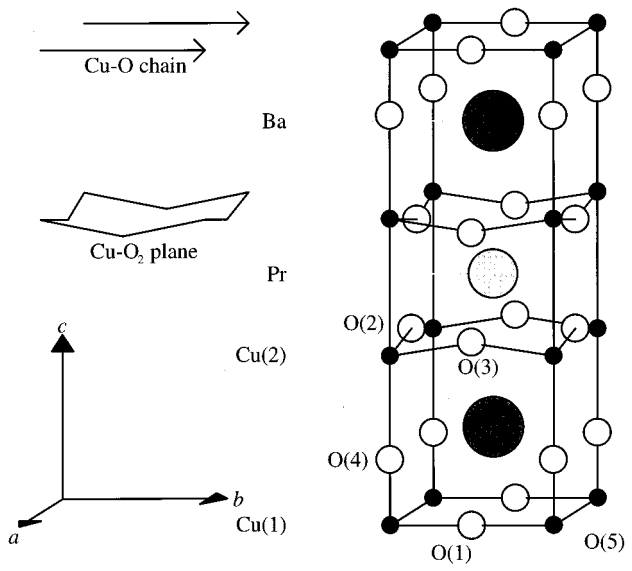

FIG. 1. The Chemical unit cell of $PrBa_2Cu_3O_7$.

In Eq. (4), the expression has been decoupled into two parts. The first factor (the ''orientation factor'') depends only on the relative orientation of the scattering vector **K** and the direction of the magnetic moments $\boldsymbol{\mu}$. The second factor contains information about the magnetic structure and is the structure factor of a collinear ordering.

Equations (1) and (4) have units of μ_B^2, and all measured intensities were normalized to these units by comparison with nuclear reflections. For the calculated intensities, the sums in Eqs. (1) and (4) were taken over a magnetic cell which was $2\times2\times2$ chemical unit cells. The chemical unit cell is shown in Fig. 1, and all reflections (magnetic and nuclear) are indexed with respect to this cell.

For the Cu moments, form factors corresponding to the $3d$ wave function with symmetry of the type $d_{x^2-y^2}$ were used;[20,21] for the Cu(2) moments, the axis of quantization (z) points along the c axis, whereas for the Cu(1) moments it is assumed to point along the a axis. Linear radial expansions or contractions of the free-ion wave function were permitted, to allow for the effects of the crystalline environment.

For the Pr moments, the dipole approximation was used in calculating the magnetic form factor. We assumed the ions are in a Pr^{3+} valence state ($S=1$, $L=5$, $J=4$).

In calculating the intensities, the resolution of the triple-axis spectrometer and the intrinsic shape of the scattering were taken into account as described in the Appendix.

V. RESULTS

We will consider the magnetic ordering phenomena observed in the oxygenated and reduced crystals separately.

A. Oxygenated crystal

The oxygenated crystal ordered into the type-I phase with a Néel temperature of $T_N\approx360$ K. This is a simple, collinear, antiferromagnetic ordering of the Cu(2) moments, as shown in Fig. 2. The structure factor from Eq. (2) is

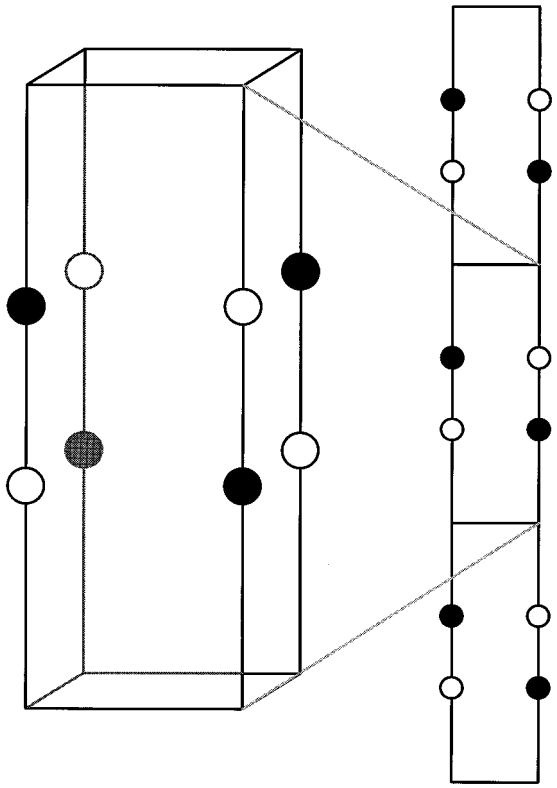

FIG. 2. Cu type-I ordering.

$$F^{\alpha}(\mathbf{K}) = 16i\mu^{\alpha}_{\mathrm{Cu}(2)} f_{\mathrm{Cu}(2)}(\mathbf{K})\sin(2\pi lz), \tag{5}$$

where z is the fractional height of the Cu(2) moment from the basal plane. The magnetic moments lie parallel to the ab plane, but because of domain averaging the absolute orientation of the Cu moments within the plane does not affect the Bragg intensities and so cannot be determined. Reflections occur at $(h+\frac{1}{2},k+\frac{1}{2},l)$, where h,k,l are integers and $l\neq0$. [The $l=0$ reflection does not occur due to the sinusoidal structure factor, Eq. (5).]

The intensities measured at 40 K are given in Table IV. These intensities correspond to a measured Cu(2) moment of $\mu_{\mathrm{Cu}(2)}=(0.493\pm0.010)\mu_B$. The fitted form factor indicated a radial contraction (compared to the calculated free-ion wave functions) of $\beta=(22\pm2)\%$.

TABLE IV. Observed and fitted intensities for the oxygenated crystal in the Cu type-I phase at 40 K.

(h,k,l)	I_{obs}/μ_B^2	I_{fit}/μ_B^2
$\frac{1}{2},\frac{1}{2},1$	21.4±0.2	21.4
$\frac{1}{2},\frac{1}{2},2$	36.0±0.4	36.0
$\frac{1}{2},\frac{1}{2},3$	3.9±0.2	4.0
$\frac{1}{2},\frac{1}{2},4$	15.8±0.4	15.6
$\frac{1}{2},\frac{1}{2},5$	42.9±0.7	43.3
$\frac{1}{2},\frac{1}{2},6$	14.4±0.6	13.9
$\frac{1}{2},\frac{1}{2},7$	4.0±0.6	3.9
$\frac{3}{2},\frac{3}{2},1$	8.1±0.6	8.6
$\frac{3}{2},\frac{3}{2},2$	12.5±0.7	12.4
$\frac{3}{2},\frac{3}{2},3$	2.8±0.7	1.3
		$\chi^2=1.0$

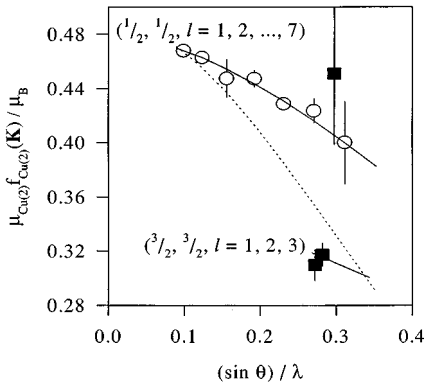

FIG. 3. Experimental and calculated Cu(2) form factors for the oxygenated crystal in the Cu type-I phase at 40 K. Open circles represent the $h=\frac{1}{2}$ series; solid squares represent the $h=\frac{3}{2}$ series. The solid line shows the $d_{x^2-y^2}$ symmetry, whereas the dotted line shows the d_{r^2} symmetry.

To demonstrate the anisotropy of the $d_{x^2-y^2}$ symmetry and the necessity of using this symmetry, we show in Fig. 3 the variation of $\mu f(\mathbf{K})$ with $(\sin\theta)/\lambda$. The experimental data are in much better agreement with the $d_{x^2-y^2}$ symmetry than the spherical symmetry, as observed previously.[22] The χ^2 of the fit using the spherical form factor is 24.

Figure 4 shows the intensity of one of the type-I phase reflections, the $(\frac{1}{2},\frac{1}{2},2)$, as a function of temperature. At a temperature of approximately 11 K, there is a sudden decrease in intensity. This corresponds to a change in the Cu magnetic structure and also coincides with the development of a new magnetic phase which, as we show later, involves Pr ordering. At this temperature the magnetic structure of the Cu moments turns into the intermediate phase of the type-II Cu structure. This is a noncollinear ordering which involves a rotation of alternating bilayers of Cu(2) moments in opposite directions, as shown in Fig. 5. The direction of the moments remains in the ab plane, and when the rotation is complete ($\phi=90°$), a state not reached in the oxygenated crystal, the moments are once again in a collinear arrangement (the type-II ground state). The type-I magnetic structure has a period c, and so reflections are observed for $l=1,2,3,\ldots$. In the type-II intermediate phase, the components of the moments parallel to $\phi=0$ have period c, whereas the components perpendicular to $\phi=0$ have period $2c$. For this reason, reflections are seen both at $l=1,2,3,\ldots$ and $l=\frac{1}{2},\frac{3}{2},\frac{5}{2},\ldots$. Finally, in the type-II ground state, if it occurs, the magnetic structure only has a periodicity of $2c$, and so reflections are observed only at $l=\frac{1}{2},\frac{3}{2},\frac{5}{2},\ldots$.

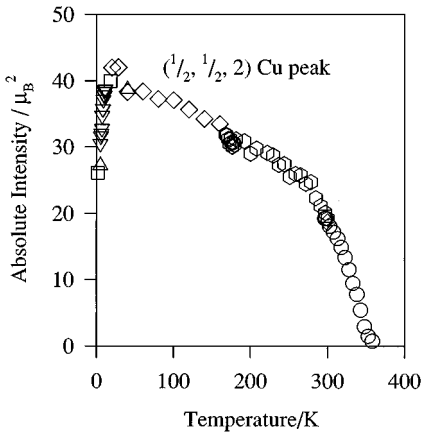

FIG. 4. Intensities of the $(\frac{1}{2},\frac{1}{2},2)$ reflection of the oxygenated crystal as a function of temperature. The data are a combination of several runs as indicated by the symbols. The systematic uncertainty in the absolute intensity is approximately 8%.

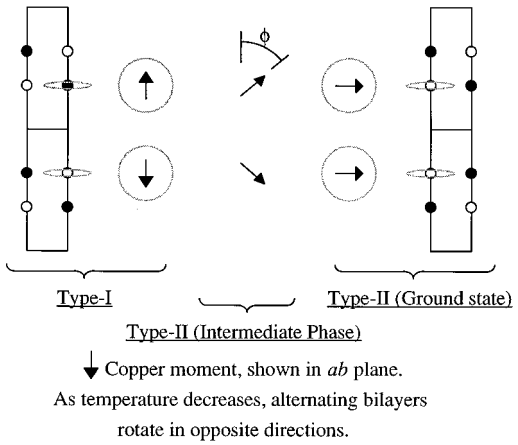

FIG. 5. Transition from Cu type-I to type-II ordering via the intermediate phase.

On previous occasions when the type-II ordering has been observed in $R\mathrm{Ba_2Cu_3O_{6+x}}$, it has often been reported that there is an additional antiferromagnetic ordering of the sublattice of Cu(1) moments, along the line $\phi=90°$. Reports differ as to whether the coupling with the adjacent Cu(2) moments is ferromagnetic[23] or antiferromagnetic,[24] and the size of the Cu(1) moments also varies greatly. We could not tell whether or not there were ordered moments on the Cu(1) ions in the oxygenated crystal as the intermediate phase had only just developed, and so the $l+\frac{1}{2}$ reflections were still weak at the lowest temperatures attainable. The type-II ground state (Fig. 6) is not attained as $T\rightarrow 0$ K.

The second magnetic phase which developed at around 11 K was also characterized by reflections at $(h+\frac{1}{2},h+\frac{1}{2},l)$, $l=$integer, but with the difference that $l=0$ was a strong reflection. These new peaks were significantly broader in the l direction than the experimental resolution and Lorentzian in shape, but in the hh direction they were resolution limited. The extent of this broadening is illustrated by the surface/contour plot of the $(\frac{1}{2},\frac{1}{2},0)$ peak shown in Fig. 7.

Although the peaks showed only imperfect long-range order in the c direction (demonstrated by the existence of broadening along l), we shall refer to them as three dimensional (3D). By this we do not mean that the ordering is driven by an interaction which is strongly three dimensional in character, but only that the resulting structure showed order in three dimensions—hence, we observe (3D) Bragg peaks, not the (2D) Bragg rods which would occur if there were no order in the third dimension. We make this point to avoid the confusion that has, on occasion, occurred in the past.[25]

The intrinsic width [half width at half maximum (HWHM)] in the c direction of this Lorentzian peak (after accounting for resolution effects) at 1.6 K is 0.029 ± 0.002 $\mathrm{Å}^{-1}$. As stated earlier, the Cu ordering should give no reflec-

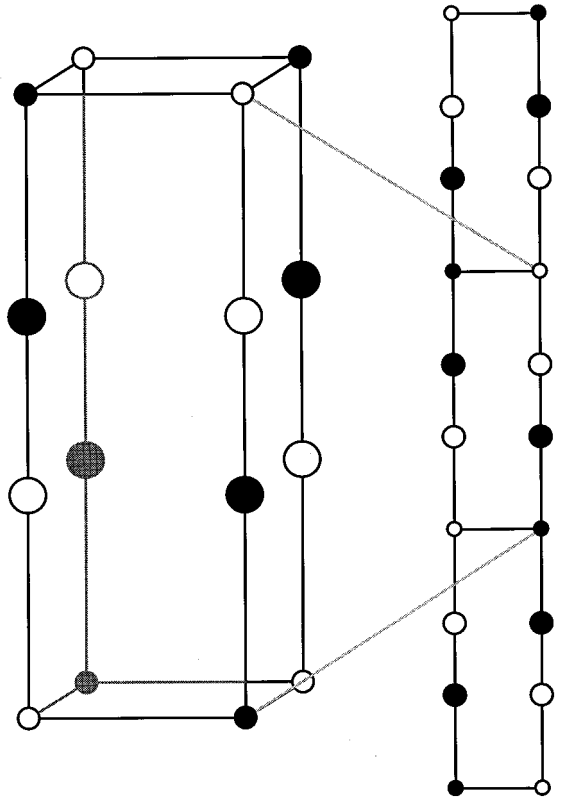

FIG. 6. Cu type-II ground state, showing the case when the Cu(1) moments are coupled ferromagnetically to the adjacent Cu(2) moments.

tion at $l=0$: The Cu(2) moments cannot contribute at $l=0$ due to the bilayer structure factor, Eq. (5), and the antiferromagnetic sublattice of the Cu(1) moments only contributes to $l+\frac{1}{2}$ (l=integer) reflections. The $(\frac{1}{2},\frac{1}{2},0)$ peak, therefore, must originate from magnetic ordering of the Pr sublattice. Although the Pr and Cu type-II orderings commence at the same temperature in the Oxford oxygenated crystal, we do not believe that the phases are necessarily coupled. In our other oxygenated crystal, the Århus crystal, the Pr ordered phase was observed to commence without the presence of the Cu type-II phase.

Having established that, at low temperatures, both Cu and Pr ordering can coexist and that both phases produce reflections $(h+\frac{1}{2},h+\frac{1}{2},l)$, we need to account for the two contributions in the analysis of the intensities.

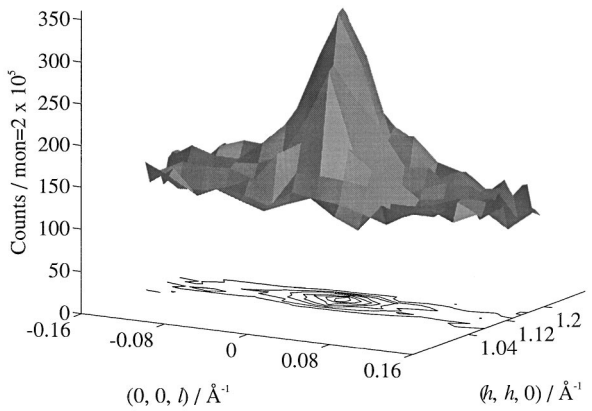

FIG. 7. Peak at $(\frac{1}{2},\frac{1}{2},0)$ in the oxygenated crystal at 1.6 K.

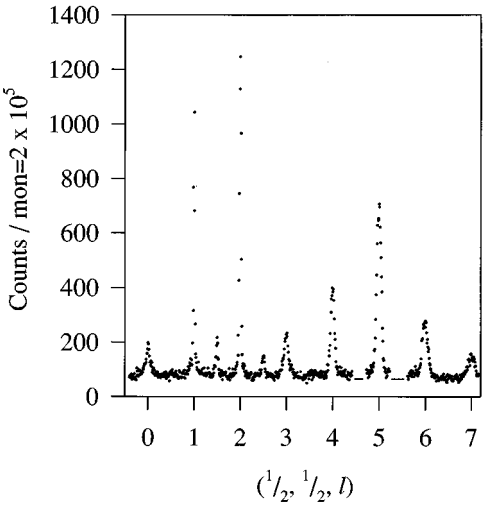

FIG. 8. l scan measured on the oxygenated crystal at 1.6 K, showing the Cu reflections at l and $l-\frac{1}{2}$ (l=integer, >0) and also the Pr reflections at l (l=integer). Aluminum powder lines around $l=4.5$ and 5.5 have been removed for clarity. The counting time per point (a monitor count of 2×10^5) was approximately 50 s.

This procedure is simplified if we note that, as long as the orderings of the contributing moments within the Cu and Pr sublattices are separately collinear, the geometric parts of their structure factors are 90° out of phase. From Eq. (2), the combined structure factor then has the form $F^{\alpha}(\mathbf{K})=F^{\alpha}_{\mathrm{Pr}}+iF^{\alpha}_{\mathrm{Cu}}$, where F^{α}_{Cu} and F^{α}_{Pr} are real (with our choice of axes). It then follows that $I(\mathbf{K})=I_{\mathrm{Cu}}(\mathbf{K})+I_{\mathrm{Pr}}(\mathbf{K})$ because all the cross terms $F^{\alpha}_{\mathrm{Pr}}F^{\beta}_{\mathrm{Cu}}$ and $F^{\beta}_{\mathrm{Pr}}F^{\alpha}_{\mathrm{Cu}}$ in Eq. (1) vanish. Hence the Cu and Pr contributions add as *intensities*, not *amplitudes*.

To obtain detailed information on the simultaneous ordering of the Cu and Pr moments, we performed two wide scans at a temperature of 1.6 K parallel to l: $(\frac{1}{2},\frac{1}{2},l)$ over the range $-0.4\leqslant l\leqslant 7.2$ and $(\frac{3}{2},\frac{3}{2},l)$ for $-0.4\leqslant l\leqslant 2.3$. Figure 8 shows the complete scan along the $(\frac{1}{2},\frac{1}{2},l)$ direction. The ordering was also investigated via scans performed parallel to $(h,h,0)$.

During the analysis of these scans, however, we found evidence for a continuous ridge of magnetic scattering parallel to l over the entire $(\frac{1}{2},\frac{1}{2},l)$ scan. Figure 9 shows scans parallel to $(h,h,0)$ and $(0,0,l)$ centered on $(\frac{1}{2},\frac{1}{2},6.5)$ which clearly show this ridge.

This ridge is much more intense than can be accounted for by the tails of the surrounding Lorentzians from the Pr ordering (by a factor of at least 20). Furthermore, the ridge was only observed at temperatures below 5 K, and so it does not appear to correlate with either the onset of the type-II Cu ordering or the Pr ordering. Within error, there is no evidence for any intrinsic width in the hh direction. Since the Cu(2) moments are already strongly ordered and the Pr moments order at about 11 K, it seems most likely that this is a Bragg rod arising from a two-dimensional (2D) ordering of the Cu(1) moments within the basal plane of the unit cell. We would also expect a $(\frac{3}{2},\frac{3}{2},l)$ ridge to exist, and although we

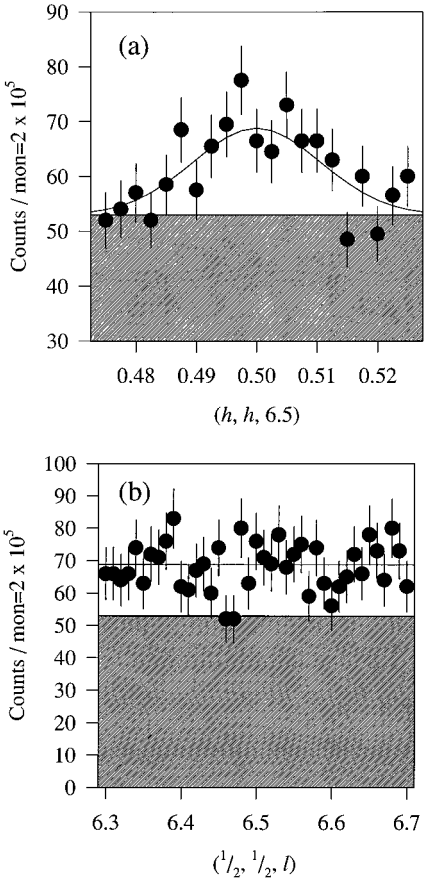

FIG. 9. (a) hh and (b) l scans through the $(\frac{1}{2},\frac{1}{2},6.5)$, showing the existence of a ridge of scattering along l. Only about 3% of this ridge can be attributed to Lorentzian tails. The width [full width at half maximum (FWHM)] of the rod in the $(h,h,0)$ direction, $\Delta h = 0.025 \pm 0.006$, is comparable to the calculated resolution width of 0.020. The shaded region is the background.

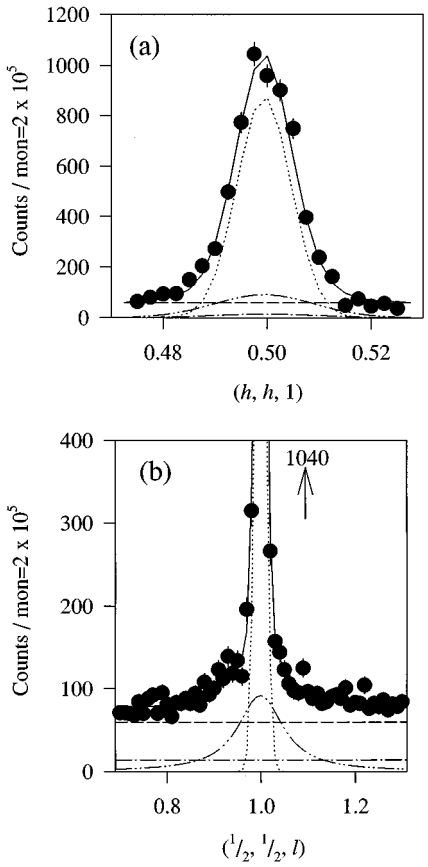

FIG. 10. Fits for the (a) hh scan and (b) l scan through the position $(\frac{1}{2},\frac{1}{2},1)$, measured at 1.6 K. The individual contributions are (dashed line) flat background, (dot-dashed line) 2D ridge, (double-dot-dashed line) Pr peak, (dotted line) Cu peak, and (solid line) total.

did not perform scans specifically to investigate it, our measurements indicated that, if the ridge exists, it is much weaker than the $(\frac{1}{2},\frac{1}{2},l)$ ridge.

Summarizing, at 1.6 K we observed sharp reflections from 3D Cu ordering, Lorentzian peaks from Pr ordering, and a diffuse ridge of scattering parallel to l underneath all the other magnetic peaks. Unfortunately, during the experiment itself, the ridge was not recognized, and so we have no scans across the ridge at noninteger or half-integer l positions. Hence we fitted the data, taking proper account of the resolution and the intrinsic scattering functions (see the Appendix), according to the following procedure.

(i) The intensities of the $(\frac{1}{2},\frac{1}{2},l)$ and $(\frac{3}{2},\frac{3}{2},l)$ ridges were determined at various points along their length from some of the hh and l scans. The scans used for this purpose were those that contained intensity from only one type of 3D ordering and so were the simplest to analyze. The observed ridge intensities were modeled as described below, and for the remaining analysis the ridge intensity was calculated from the model and treated as a fixed parameter.

(ii) The intrinsic widths of all the Pr Lorentzian peaks were assumed to be the same as the intrinsic width determined from the $(\frac{1}{2},\frac{1}{2},0)$ reflection by taking into account the resolution (see the Appendix).

(iii) We were able to isolate accurately the Cu contribution from the Pr contribution for the two reflections $(\frac{1}{2},\frac{1}{2},1)$ and $(\frac{1}{2},\frac{1}{2},2)$, where the resolution was most favourable (see Fig. 10). These Cu intensities, together with those at $(\frac{1}{2},\frac{1}{2},\frac{3}{2})$ and $(\frac{1}{2},\frac{1}{2},\frac{5}{2})$, then allowed us to establish the Cu(2) moment and the turn angle ϕ.

(iv) The Cu contributions to the other $(\frac{1}{2},\frac{1}{2},l)$ and $(\frac{3}{2},\frac{3}{2},l)$ reflections at 1.6 K were deduced by scaling the reflections measured at 18 K (above the temperature for the Pr and ridge scattering) to match the $(\frac{1}{2},\frac{1}{2},1)$ and $(\frac{1}{2},\frac{1}{2},2)$ Cu intensities at 1.6 K previously found.

(v) Finally, with the Cu and ridge intensities known, the Pr intensities of the peaks were determined.

We will discuss first the intensities obtained for the ridges. Table V gives the ridge intensity at 1.6 K for each position where it was determined.

These small intensities are very difficult to measure and for the $h=\frac{3}{2}$ series were beyond the sensitivity of our measurements. For the $h=\frac{1}{2}$ series, there is also no modulating factor, implying that all the correlations are within one layer. As discussed above, it seems most likely that the ridges of scattering arose from 2D antiferromagnetic ordering of the Cu(1) moments in the ab plane. Using this model we calculated the intensities $I_{\rm fit}$ given in Table V. The calculated and observed intensities agree quite well, and the Cu(1) moment, assumed to be in the ab plane, was found to be $\mu_{\rm Cu(1)}=(0.32\pm0.04)\mu_B$ within this model. [The mean mo-

TABLE V. Intensity of the diffuse ridges of scattering at 1.6 K. I_{obs} is the measured intensity obtained from hh and l scans through the (h,k,l) positions given. I_{fit} is the intensity calculated from the model described in the text.

(h,k,l)	I_{obs}/μ_B^2	I_{fit}/μ_B^2
$\frac{1}{2},\frac{1}{2},0$	1.2±0.3	0.9
$\frac{1}{2},\frac{1}{2},\frac{1}{2}$	1.1±0.3	1.0
$\frac{1}{2},\frac{1}{2},\frac{3}{2}$	1.4±0.2	1.2
$\frac{1}{2},\frac{1}{2},\frac{5}{2}$	0.8±0.2	1.2
$\frac{1}{2},\frac{1}{2},\frac{7}{2}$	1.3±0.5	1.1
$\frac{1}{2},\frac{1}{2},\frac{13}{2}$	1.2±0.4	0.5
$\frac{3}{2},\frac{3}{2},0$	0.4±0.4	0.5
$\frac{3}{2},\frac{3}{2},\frac{1}{2}$	0.2±0.3	0.5
$\frac{3}{2},\frac{3}{2},\frac{3}{2}$	0.2±0.3	0.4
		$\chi^2=1.5$

ment per Cu(1) site was $(0.18\pm0.02)\mu_B$—the value of $\mu_{Cu(1)}$ reflects the occupancy of this site by actual Cu(1) ions.]

Next we consider the measured and fitted Cu intensities of the type-II intermediate phase at 1.6 K. These are given in Table VI, and correspond to a Cu(2) moment of $\mu_{Cu(2)}=(0.45\pm0.03)\mu_B$, with a turn angle of $\phi=(19.1\pm0.3)°$. We could not ascertain whether or not there was a small three-dimensionally ordered moment on the Cu(1) sites from this limited data set, but this would be unlikely if the Cu(1) moments were already ordered in two dimensions as suggested by the diffuse scattering ridge.

Finally, we list in Table VII the intensities deduced for the Pr components to the peaks. We initially fitted the intensities assuming the Pr moments to be pointing along the c axis ($\theta=0$), as has been previously suggested.[4] As can be seen from Table VII, however, this model does not give a good fit to the experimental data ($\chi^2=32$). As $|\mathbf{K}|$ increases, the orientation factor suppresses the model intensities much more quickly than the observed intensities. We then allowed the Pr moments to point at an angle θ away from the c axis, and much better agreement was obtained. The best fit gave $\mu_{Pr}=(0.50\pm0.04)\mu_B$, $\theta=(59\pm3)°$, with a χ^2 of 3.8.

Any remaining discrepancies between the data and the fit could be caused by the true form factor of the Pr moments not being the same as that predicted by the dipole approximation due to, for example, hybridization or crystal-field effects.

We cannot determine the absolute orientation ϕ of the Pr moments within the ab plane. We can determine, however, that they are collinear, since reflections are only seen at integer l. The model for the Pr ordering in this crystal is illustrated in Fig. 11.

TABLE VI. Measured and fitted Cu intensities at 1.6 K of those peaks where the Cu contribution is easily resolvable from other features.

(h,k,l)	I_{obs}/μ_B^2	I_{fit}/μ_B^2
$\frac{1}{2},\frac{1}{2},1$	15.9 ±0.3	15.6
$\frac{1}{2},\frac{1}{2},2$	26.1 ±0.4	26.3
$\frac{1}{2},\frac{1}{2},\frac{3}{2}$	2.87±0.13	3.12
$\frac{1}{2},\frac{1}{2},\frac{5}{2}$	2.32±0.14	1.85

TABLE VII. Measured and fitted Pr intensities at 1.6 K. θ is the angle of the Pr moment away from the c axis.

(h,k,l)	I_{obs}/μ_B^2	$I_{\theta=0}/\mu_B^2$	$I_{\theta=59°}/\mu_B^2$
$\frac{1}{2},\frac{1}{2},0$	12.8±1.3	12.7	9.4
$\frac{1}{2},\frac{1}{2},1$	10.6±1.2	10.2	9.5
$\frac{1}{2},\frac{1}{2},2$	11.4±1.2	6.3	9.6
$\frac{1}{2},\frac{1}{2},3$	9.0±0.7	3.7	9.4
$\frac{1}{2},\frac{1}{2},4$	7.2±0.8	2.3	8.9
$\frac{1}{2},\frac{1}{2},5$	8.7±1.6	1.4	8.1
$\frac{1}{2},\frac{1}{2},6$	8.0±0.8	0.9	7.3
$\frac{1}{2},\frac{1}{2},7$	7.8±0.9	0.6	6.4
$\frac{3}{2},\frac{3}{2},0$	7.2±0.8	8.6	6.4
$\frac{3}{2},\frac{3}{2},1$	3.8±0.7	8.3	6.3
$\frac{3}{2},\frac{3}{2},2$	8.2±1.2	7.5	6.3
		$\chi^2=32$	$\chi^2=3.8$

The intensities of reflections characteristic of these differing low-temperature magnetic structures were followed with temperature, and these are plotted in Fig. 12.

B. Reduced crystal

The reduced crystal was found to exhibit substantial differences in the Cu and Pr ordering compared to the oxygenated crystal. Figure 13 shows the temperature dependence of the $(\frac{1}{2},\frac{1}{2},2)$ intensity. The crystal orders into the Cu type-I phase at 370 K and then enters into the type-II intermediate phase at 100 K.

To check the model for the intermediate phase, we measured sets of reflections at two different temperatures 30 and 57.5 K. Table VIII lists the observed and fitted intensities measured at 30 K, a temperature which is approximately midway between the Cu type-I and type-II ground states. The intensities were fitted both with and without a moment on the Cu(1) site present. A slight improvement to the fit was made by including the moment, and this fit is given in Table VIII.

The results of the fit for data taken at 30 K were a Cu(2) moment of $\mu_{Cu(2)}=(0.57\pm0.06)\mu_B$, a Cu(1) moment of $\mu_{Cu(1)}=(0.039\pm0.014)\mu_B$ (assuming the same amount of vacancies and Al contamination as in the Oxford oxygenated crystal), a turn angle of $\phi=(48.5\pm0.5)°$, and a radial contraction of $\beta=(17\pm3)\%$ in the Cu(2) ion wave function. In

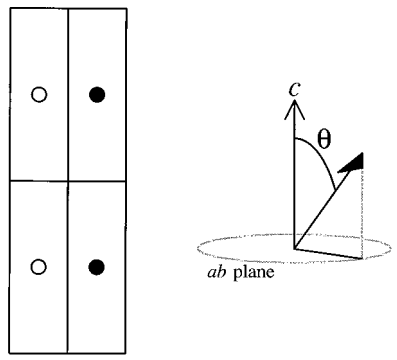

FIG. 11. Pr ordering. The moments exist in a $(\frac{1}{2},\frac{1}{2},0)$ magnetic structure, pointing at an angle θ away from the c axis. All the moments have the same ϕ orientation.

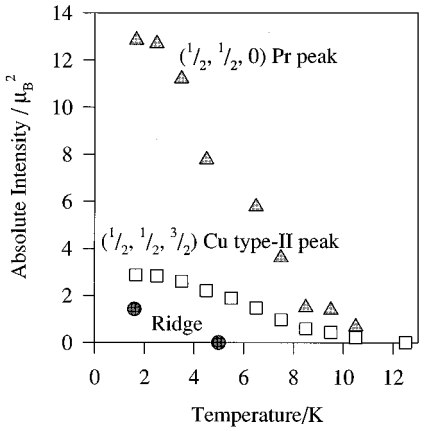

FIG. 12. Intensities of characteristic reflections of the low-temperature phases of the oxygenated crystal as a function of temperature; the ridge intensity was measured at the $(\frac{1}{2},\frac{1}{2},0)$ position. The systematic errors in the absolute intensities are about 10%.

view of the results found at lower temperatures (see below), we believe the nonzero Cu(1) moment is a genuine effect. The moment is coupled *ferromagnetically* to the Cu(2) moments above and below it, as illustrated in Fig. 6.

At 57.5 K, the fit gave $\mu_{\mathrm{Cu}(2)}=(0.57\pm0.05)\mu_B$, $\phi=(29.8\pm1.2)°$, and $\beta=(25\pm3)\%$. There was not enough data at 57.5 K to determine safely whether or not there was a small moment on the Cu(1) ions. This fit had a χ^2 of 1.2.

In contrast to the oxygenated crystal, in the reduced crystal the Cu type-II ground state ($\phi=90°$) was reached (as can be seen in Fig. 13). Table IX lists the observed and fitted intensities of the type-II ground state at 4.2 K. The fit gave $\mu_{\mathrm{Cu}(2)}=(0.59\pm0.05)\mu_B$, $\mu_{\mathrm{Cu}(1)}=(0.042\pm0.011)\mu_B$, and $\beta=(14\pm5)\%$. If the Cu(1) moment is constrained to be zero, then a much worse fit ($\chi^2=6.7$) is obtained.

We observed no 3D ordering of the Pr moments in the reduced crystal. Below about 8 K, however, we did observe a ridge of scattering indicative of 2D order. Figure 14 shows the scattering around the $(\frac{1}{2},\frac{1}{2},0)$ position at 1.7 K. There is no 3D Bragg peak centered on $(\frac{1}{2},\frac{1}{2},0)$, but the ridge is clearly

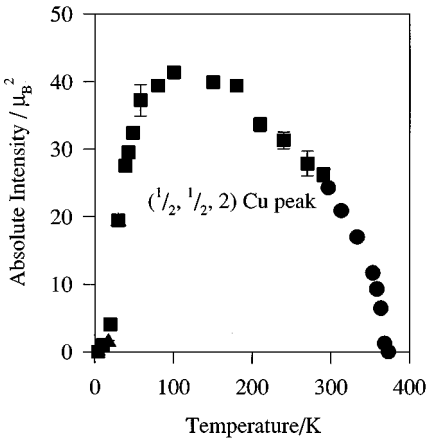

FIG. 13. Intensities of the $(\frac{1}{2},\frac{1}{2},2)$ reflection as a function of temperature. The data are a combination of several runs as indicated by the symbols. The systematic uncertainty in the absolute intensity is approximately 12%.

TABLE VIII. Observed and fitted intensities at 30 K in the type-II intermediate phase of the reduced crystal.

(h,k,l)	I_{obs}/μ_B^2	I_{fit}/μ_B^2
$\frac{1}{2},\frac{1}{2},1$	11.3±0.5	12.8
$\frac{1}{2},\frac{1}{2},2$	19.3±1.4	21.6
$\frac{1}{2},\frac{1}{2},3$	2.5±0.5	2.6
$\frac{1}{2},\frac{1}{2},4$	9.3±0.6	8.8
$\frac{1}{2},\frac{1}{2},5$	27.7±0.8	25.6
$\frac{1}{2},\frac{1}{2},6$	9.7±0.8	8.8
$\frac{3}{2},\frac{3}{2},1$	4.8±0.7	4.7
$\frac{3}{2},\frac{3}{2},2$	5.6±0.7	6.9
$\frac{1}{2},\frac{1}{2},\frac{1}{2}$	5.2±0.2	5.1
$\frac{1}{2},\frac{1}{2},\frac{3}{2}$	25.9±1.2	25.8
$\frac{1}{2},\frac{1}{2},\frac{5}{2}$	17.0±0.8	17.4
$\frac{1}{2},\frac{1}{2},\frac{9}{2}$	27±3	24.8
$\frac{1}{2},\frac{1}{2},\frac{11}{2}$	20±6	26.8
$\frac{3}{2},\frac{3}{2},\frac{3}{2}$	8.4±0.7	8.7
$\frac{3}{2},\frac{3}{2},\frac{5}{2}$	5.8±0.7	5.4
		$\chi^2=2.7$

seen in the hh scans through $l=0$ and $l=\frac{1}{4}$. The l scan shows that the ridge is essentially flat in this small region.

As discussed above, the ridge of scattering which we observed in the oxygenated crystal seemed to arise from a 2D ordering of Cu(1) moments. In the reduced crystal, however, it seems more likely that the ridge is being caused by a 2D ordering of the Pr moments. We base this deduction on three observations: (i) the absence of any 3D Pr ordering in this crystal, (ii) the apparent existence of a 3D ordered Cu(1) moment up to temperatures at least as high as 30 K, and (iii) the manner in which the ridge intensity falls off in l, as we now discuss.

Even though the rod is flat in the small region shown in Fig. 14(b), you would expect a variation with **K** due to the form factor and the orientation factor [see Eq. (4)].

Table X shows some measurements of the ridge intensity at different values of l at a temperature of 1.5 K. The direction of the ordered moment has a strong influence, through the orientation factor, on the **K** dependence of the ridge intensity. The intensities in Table X have been fitted with the assumption that the ordered moment is from the Pr sublattice and that it points along the c axis. The close agreement with the observed intensities supports these assumptions. Since we expect the Cu(2) moments to lie in the ab plane, it is unlikely that the ridge of scattering could arise from 2D *copper* ordering.

TABLE IX. Observed and fitted intensities of the type-II ground state for the reduced crystal at 4.2 K.

(h,k,l)	I_{obs}/μ_B^2	I_{fit}/μ_B^2
$\frac{1}{2},\frac{1}{2},\frac{1}{2}$	9.0±0.3	8.9
$\frac{1}{2},\frac{1}{2},\frac{3}{2}$	46.7±0.8	47.0
$\frac{1}{2},\frac{1}{2},\frac{5}{2}$	33.0±0.9	33.2
$\frac{1}{2},\frac{1}{2},\frac{9}{2}$	42.6±1.3	41.8
$\frac{1}{2},\frac{1}{2},\frac{13}{2}$	4.2±0.9	3.4
$\frac{3}{2},\frac{3}{2},\frac{3}{2}$	13.5±1.7	14.2
		$\chi^2=0.8$

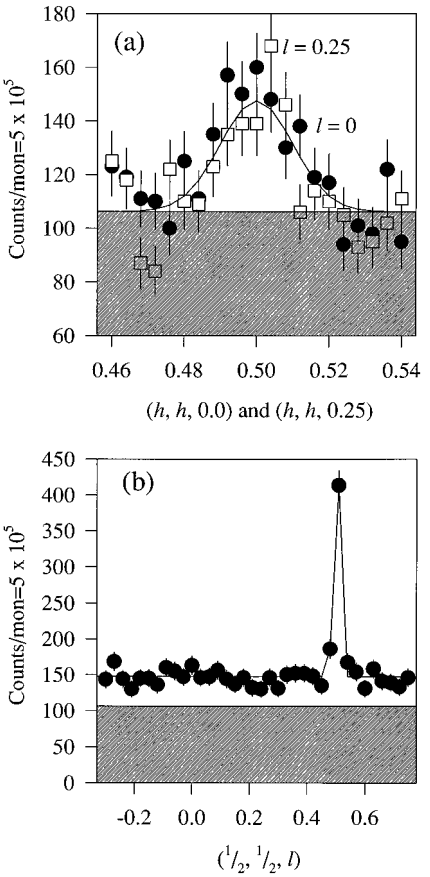

FIG. 14. (a) hh and (b) l scans of the ridge in the reduced crystal at 1.7 K. The peak at $l=\frac{1}{2}$ in (b) is a Cu type-II ground-state reflection. The shaded region is the background.

Our conclusion is that the ridge of scattering is caused by a 2D antiferromagnetic ordering of the Pr moments, with the moment direction along the c axis. The magnitude of the ordered moment at 1.5 K is $\mu_{\mathrm{Pr}}=(0.31\pm0.05)\mu_B$, but it may not have reached its fully ordered value.

The intensities of reflections characteristic of the two different magnetic structures observed at low temperatures in the reduced crystal are shown in Fig. 15.

Below 15 K, the Cu type-II reflections show a reduction in intensity as temperature decreases. As both the $(\frac{1}{2},\frac{1}{2},\frac{3}{2})$ and the $(\frac{1}{2},\frac{1}{2},\frac{5}{2})$ reflections show this effect, the decrease cannot be the result of the Cu(1) moment increasing and combining destructively with the Cu(2) moment (if this were the case, then one reflection would increase in intensity while the other decreased). We conclude that the Cu(2) moment decreases in magnitude below 15 K. This may be due to some interaction with the 2D ordering of the Pr ions which is causing the ridge intensity.

TABLE X. Intensity of the ridge of scattering in the reduced crystal at 1.5 K. I_{fit} is the calculated intensity assuming a 2D ordering of the Pr moments.

(h,k,l)	I_{obs}/μ_B^2	I_{fit}/μ_B^2
$\frac{1}{2},\frac{1}{2},\frac{3}{2}$	4.9±1.4	3.7
$\frac{1}{2},\frac{1}{2},2$	2.6±0.9	2.9
$\frac{1}{2},\frac{1}{2},\frac{5}{2}$	1.8±0.8	2.3
		$\chi^2=0.55$

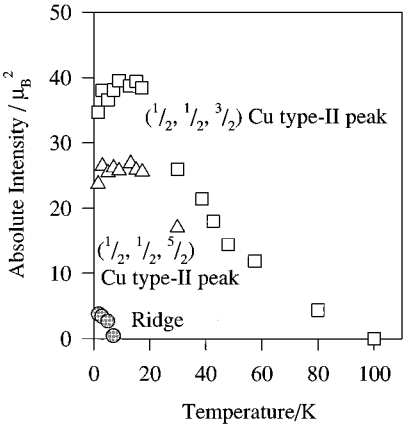

FIG. 15. Intensities of characteristic reflections of the low-temperature phases of the reduced crystal as a function of temperature; the ridge intensity was measured at the $(\frac{1}{2},\frac{1}{2},0)$ position. The systematic errors in the absolute intensities are about 11%.

VI. DISCUSSION

Varying the amount of oxygen in the samples has a significant effect on the ordering observed at low temperatures. Table XI summarises the onset temperatures of the various phases observed in the oxygenated and reduced crystals.

A. Pr ordering

In this paper we present a single-crystal neutron diffraction determination of the magnetic ordering of the praseodymium sublattice. Our results differ from those obtained previously by other methods in a number of ways, and it is perhaps best to consider these differences in turn.

First, we find that, in our oxygenated crystal, the magnetic moments, though collinear, are tilted away from the c axis by an angle $\theta=(59\pm3)°$. This result has been established on the basis of 11 different magnetic reflections. Neutron scattering has been performed previously on oxygenated *powder* samples,[4] but in this case there were only two resolvable peaks and the spin direction of the moments could only be ''tentatively'' assigned to the c axis, i.e., $\theta=0$. Interestingly, if we only look at our two strongest Pr peaks, the $(\frac{1}{2},\frac{1}{2},0)$ and

TABLE XI. Onset temperatures of the various proposed magnetic structures in the oxygenated and reduced crystals.

Magnetic phase	Oxygenated (K)	Reduced (K)
Cu type I	360	370
Cu type II (intermediate)	11	100
Cu type II (ground state)		5
Cu(1) 2D ordering?	3–4	
Pr 3D ordering	11	
Pr 2D ordering		8

$(\frac{1}{2},\frac{1}{2},1)$, we also have good agreement for $\theta=0$; it is the inclusion of the weaker reflections which reveals the nonzero value of θ.

However, our result is not completely isolated. Hodges *et al.*[26] have performed $^{170}Yb^{3+}$ Mössbauer spectroscopy on polycrystalline samples, and their results also suggest that the Pr moments are aligned well away from the c axis. In fact, they were able to obtain a good fit to their data by assuming a value of $\theta\sim65°$, which is in good agreement with our value. (They obtained a slightly better fit by allowing θ to show a distribution).

It is legitimate to ask if this tilting of the Pr moments is universal in $PrBa_2Cu_3O_{6+x}$ or if it is sample dependent. As mentioned above, previous diffraction data are consistent with ours, though they suffered from a lack of resolvable peaks. However, it is worth remembering that the easy moment direction is determined by the crystal-field levels, which may be influenced by impurities or oxygen content. The lowest crystal-field levels of $PrBa_2Cu_3O_{6+x}$ consist of a closely spaced quasitriplet of states, which may be susceptible to subtle chemical changes.

A moment direction away from the c axis may also provide an explanation as to why the Pr peaks are broadened along the c axis even at 1.6 K. It would seem likely that there would exist different ϕ positions degenerate in energy, and so the structure may involve spin domains with different ϕ orientations. These domains would be layered: strongly correlated in the ab plane, but with a short coherence length of $1/(0.029\pm0.002)=(34\pm3)$ Å in the c direction.

A further difference between our results and those previously reported for the Pr structure in oxygenated samples is that we observe ferromagnetic coupling along the c axis; i.e., the propagation vector is $(\frac{1}{2},\frac{1}{2},0)$, whereas in powders[4] it has been observed to be antiferromagnetic; i.e., the propagation vector is $(\frac{1}{2},\frac{1}{2},\frac{1}{2})$. However, examples of different couplings in samples containing the same rare-earth ions (for example, Er) are not unusual.[27] It is probable that, in our case, the superexchange has been influenced by the Al substitution at the Cu(1) site. Li *et al.*[28] have shown that doping Zn onto the Cu(2) site in $PrBa_2Cu_3O_{6+x}$ also changes the coupling along c to be ferromagnetic.

Aluminum substitution is also probably responsible for the depression of our 3D Pr Néel temperatures T_{Pr}, which have previously been found to be about 17 K in oxygenated samples[3–5] and 11 K in reduced samples.[10] Again, this shows the influence of Al on the superexchange: We observed 11 K in our oxygenated crystal and no 3D Pr ordering in our reduced crystal. Substitution of Fe and Ni onto the Cu(1) site has also been shown to reduce T_{Pr} (Ref. 29) at a rate of $dT_{Pr}/dz\sim0.65$ K/at. % and $dT_{Pr}/dz\sim0.45$ K/at. %, respectively; the Oxford oxygenated crystal has a depression rate (with Al substitution) of $dT_{Pr}/dz\sim0.50$ K/at. %.

With the superexchange along the c axis disrupted by both the removal of oxygen and the presence of Al, the Pr sublattice in the reduced crystal is apparently able to order two dimensionally in the ab plane (i.e., with no correlations along the c axis), and hence we see Bragg rods in this crystal below about 8 K. In powder samples of $PrBa_2Cu_3O_{6.2}$, a 3D magnetic structure (coupled antiferromagnetically along the c axis) was reported,[12] but the correlation length along the c axis was found to be only ~10 Å, showing the system to be very close to 2D.

B. Cu(1) and type-II ordering

Neutron scattering studies in the past have occasionally implied that the existence of the type-II phases (i.e., intermediate and ground state) necessarily requires the presence of an ordered Cu(1) moment. However, the same types of reflections would be present whether or not the Cu(1) moment is ordered (see Fig. 5). Only a detailed analysis of the observed intensities can reveal the presence of an ordered Cu(1) moment and show how it couples to its neighbors.

Previous reports of ordering of the Cu(1) moments have been varied. The Cu(1) moments in the type-II ground state of $NdBa_2Cu_3O_{6.1,6.2}$ were found to be ordered and coupled *antiferromagnetically* to the adjacent Cu(2) moments.[24] In $YBa_2Cu_3O_{6.35}$, on the other hand, the evidence suggested a *ferromagnetic* coupling.[23] In our refinements we allowed both ferromagnetic and antiferromagnetic couplings, but the refined parameters unequivocally showed that the coupling in our reduced crystal was ferromagnetic, as found in Ref. 23. In our oxygenated crystal, the coupling could not be determined as there was no ordered Cu(1) moment within experimental error. NMR measurements on $PrBa_2Cu_3O_7$ have found *no* ordered Cu(1) moments down to 1.4 K;[9] in our oxygenated crystal, we also observed no 3D ordering involving the Cu(1) moments, though it seems likely that 2D ordering did occur. Rosov *et al.*,[13] using single crystals of $PrBa_2Cu_3O_{6+x}$, have reported the surprising result that the chain moments were not restricted to lie in the basal plane. Finally, NMR and nuclear quadrupole resonance (NQR) research on $RBa_2Cu_3O_{6+x}$ compounds suggests that there is no local magnetic fields at the Cu(1) site in pure samples,[30] though an ordered moment is produced by the substitution of just 1% of Fe for Cu(1) (Ref. 30) or by hydrogenation of the basal plane.[31]

Hence the existence and coupling of the Cu(1) moments appears to be sample dependent in some way. Indeed, the very existence of type-II orderings may depend on the presence of impurities. Recent work has shown that pure, aluminum-free $YBa_2Cu_3O_{6+x}$ samples do not exhibit the type-II phases.[32] Only further work, with more careful sample characterization, can resolve these difficulties.

C. Type-I Néel temperature

We have found that the type-I Néel temperature depends only weakly on oxygen content in $PrBa_2Cu_3O_{6+x}$, in agreement with previous powder studies[5,8] and some of the single-crystal data.[13] The absolute values for the Néel temperatures, however, are more widely distributed. We find $T_N\approx360$ and 370 K for our oxygenated and reduced crystals, respectively, compared with $T_N\approx285$ and 325 K by muon spin resonance (μSR),[8] and $T_N\approx325$ and 350 K by ^{57}Fe (10%) Mössbauer spectroscopy.[5] Again, this elevation of T_N in our crystals may be the result of the Al substitution at the Cu(1) site influencing the c-axis coupling or the charge doping level.

In summary, our single-crystal neutron diffraction studies on well-characterized, oxygenated and reduced samples of $PrBa_2Cu_3O_{6+x}$ have revealed a more complex magnetic

phase diagram of the Pr and Cu ordering than has previously been suggested. In the 3D ordered phase of the Pr sublattice, we have found the moments to be tilted away from the crystallographic c axis, we have observed different types of 2D ordering in both crystals at low temperatures, and we have discovered unusual magnetic behavior of the Cu(1) sites in the type-II phases. Measurements on purer crystals are in progress to establish which of these details are intrinsic to $PrBa_2Cu_3O_{6+x}$ and which are due to impurities on the Cu(1) sites.

ACKNOWLEDGMENTS

The authors gratefully acknowledge financial support from the EC Large Installation Programme, which enabled the experiments to be performed at the Risø National Laboratory, Denmark. The work by the staff at Risø is supported by the EC Science and Esprit programmes and the Danish Ministry of Energy. We are grateful to Per Solgaard for carrying out the ICPMS analysis at Risø and to Thomas Wolf (Karlsruhe) for supplying the Al-free crystal. We would also like to thank the technical staff at Risø for their assistance during these experiments, and G. J. McIntyre and R. A. Cowley for helpful discussions. One of us (A.L.) thanks the EPSRC for financial support.

APPENDIX

On a triple-axis spectrometer it is often convenient to perform elastic scans which are linear in reciprocal space. Lorentz factors for linear scans through Bragg peaks with no intrinsic structure have been calculated by Lebech and Nielsen[33] and by Cowley and Bates.[34]

We henceforth adopt the notation of Cooper and Nathans,[35] who derived the resolution function for a triple-axis spectrometer, and of Cowley and Bates.[34] In Ref. 34 the result for the Lorentz factor of a sharp Bragg reflection, i.e., $S(\mathbf{K}-\boldsymbol{\tau})=\delta(\mathbf{K}-\boldsymbol{\tau})$, where the function $S(\mathbf{K}-\boldsymbol{\tau})$ describes the intrinsic form of the scattering normalized to unit volume, in a crystal without mosaicity, is

$$L^{-1}=\frac{C}{N\sqrt{B_0}}\,(M_{11}\cos^2\alpha+2M_{12}\cos\alpha\,\sin\alpha+M_{22}\sin^2\alpha)^{1/2}, \tag{A1}$$

where α is the angle between $\boldsymbol{\tau}$ and the scan direction. The normalization of the Lorentz factor is different from that in Ref. 34 and has been chosen such that in the case of an open detector Eq. (A1) reduces to $L^{-1}=|\sin(\alpha+\theta)|$, which is the factor that is obtained by considering just geometrical effects. The M_{ij} and N parameters (which define the shape of the resolution ellipsoid and its normalization, respectively) are functions of θ, where 2θ is the scattering angle at the sample, but C and B_0 depend only on fixed instrument parameters.

1. Inclusion of mosaicity

If the sample mosaic spread η (standard deviation) is small ($\eta \ll 1$ rad), then the effect of sample mosaicity is to produce a Gaussian broadening of the peaks in the direction tangential to $\boldsymbol{\tau}$. It can be shown that this can then be absorbed into the resolution function via the transformations

$$N\rightarrow N\sqrt{\frac{m}{M_{22}+m}},$$

$$M_{11}\rightarrow M_{11}-\frac{M_{12}^2}{M_{22}+m}, \tag{A2}$$

$$M_{12}\rightarrow \frac{M_{12}m}{M_{22}+m},$$

$$M_{22}\rightarrow \frac{M_{22}m}{M_{22}+m},$$

where $m=1/(\eta\tau)^2$.

The Lorentz factor for the perfect Bragg peak, Eq. (A1), and the following Lorentz factors, Eqs. (A3) and (A4), can now include the effects of mosaicity by means of the transformations, Eq. (A2).

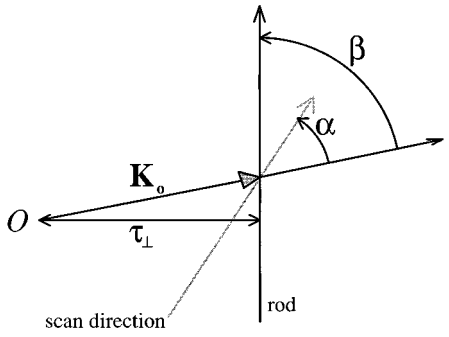

FIG. 16. Linear scan in reciprocal space. $\mathbf{K}_0$, the nominal position of the spectrometer, moves linearly along the scan direction. α defines the scan direction, and β defines the rod direction, calculated at the position when $\mathbf{K}_0$ is centered on the rod.

2. Two-dimensional structures

A two-dimensional structure comprising of ordered layers separated by a distance c gives rise to a rod of scattering in reciprocal space. Suppose that the Bragg rod lies in the scattering plane of the spectrometer. The in-plane scattering intensity can be represented by $S(\mathbf{K}-\boldsymbol{\tau})=\delta(K_\perp-\tau_\perp)c/2\pi$, where $\tau_\perp$ is the perpendicular distance from the origin to the rod in reciprocal space and $K_\perp$ is the component of $\mathbf{K}$ perpendicular to the rod in the scattering plane.

Consider a linear scan in reciprocal space such that the scan direction makes an angle $\beta-\alpha$ with the rod (see Fig. 16). The Lorentz factor for this measurement can be shown to be

$$L^{-1}=\frac{C}{Nc}\,\sqrt{\frac{2\pi}{B_0}}\,|\sin(\beta-\alpha)|\,\sqrt{M_{11}M_{22}-M_{12}^2}. \tag{A3}$$

3. Peaks with Lorentzian broadening

Suppose that we have a structure with short-range order along the c direction. If the coherence decays exponentially, then the intrinsic shape of the peak will be a Lorentzian represented by

$$S(\mathbf{K}-\boldsymbol{\tau})=\delta(K_\perp-\tau_\perp)\,\frac{\Gamma/\pi}{(K_c-\tau_c)^2+\Gamma^2},$$

where $K_\perp$ and K_c are the components of $\mathbf{K}$ perpendicular and parallel to the c direction, respectively, and similarly for $\tau_\perp$ and τ_c. This form is valid when neighboring Lorentzians do not overlap.

The Lorentz factor for this shape is found to be

$$L^{-1}=\frac{C}{N\sqrt{B_0}}\,\frac{1}{F(\alpha,\beta)}, \tag{A4}$$

where

$$F(\alpha,\beta)=\frac{1}{\sqrt{a(\alpha)}}\int_{-\infty}^{+\infty}\frac{\Gamma/\pi}{K_c^2+\Gamma^2}\times\exp\left\{-\frac{(M_{11}M_{22}-M_{12}^2)\sin^2(\beta-\alpha)}{2a(\alpha)}\,K_c^2\right\}dK_c \tag{A5}$$

and

$$a(\alpha)=M_{11}\cos^2\alpha+2M_{12}\cos\alpha\,\sin\alpha+M_{22}\sin^2\alpha. \tag{A6}$$

The cases for a perfect Bragg peak, Eq. (A1), and a Bragg rod, Eq. (A3), are the limiting forms of Eq. (A4) when $\Gamma\to 0$ and $\Gamma=2/c\gg$ resolution width, respectively.

*Present address: Department of Physics, University of Birmingham, Birmingham, B15 2TT, England.

[1] L. Soderholm, K. Zhang, D. G. Hinks, M. A. Beno, J. D. Jorgensen, C. U. Segre, and I. K. Schuller, Nature **328**, 604 (1987); J. K. Liang, X. T. Xu, S. S. Xie, X. Y. Shao, and Z. G. Duan, Z. Phys. B **69**, 137 (1987).

[2] For a full list of references to experimental work, see H. B. Radousky, J. Mater. Res. **7**, 1917 (1992).

[3] A. Kebede, C.-S. Jee, J. Schwegler, J. E. Crow, T. Mihalisin, G. H. Myer, R. E. Salomon, P. Schlottmann, M. V. Kuric, S. H. Bloom, and R. P. Guertin, Phys. Rev. B **40**, 4453 (1989).

[4] W.-H. Li, J. W. Lynn, S. Skanthakumar, T. W. Clinton, A. Kebede, C.-S. Jee, J. E. Crow, and T. Mihalisin, Phys. Rev. B **40**, 5300 (1989).

[5] I. Felner, U. Yaron, I. Nowik, E. R. Bauminger, Y. Wolfus, E. R. Yacoby, G. Hilscher, and N. Pillmayer, Phys. Rev. B **40**, 6739 (1989).

[6] J. Fink, N. Nücker, H. Romberg, M. Alexander, M. B. Maple, J. J. Neumeier, and J. W. Allen, Phys. Rev. B **42**, 4823 (1990).

[7] R. Fehrenbacher and T. M. Rice, Phys. Rev. Lett. **70**, 3471 (1993).

[8] D. W. Cooke, R. S. Kwok, M. S. Jahan, R. L. Lichti, T. R. Adams, C. Boekama, W. K. Dawson, A. Kebede, J. Schwegler, J. E. Crow, and T. Mihalisin, J. Appl. Phys. **67**, 5061 (1990).

[9] A. P. Reyes, D. E. MacLaughlin, M. Takigawa, P. C. Hammel, R. H. Heffner, J. D. Thompson, J. E. Crow, A. Kebede, T. Mihalisin, and J. Schwegler, Phys. Rev. B **42**, 2688 (1990).

[10] A. Kebede, J. P. Rodriquez, I. Perez, T. Mihalisin, G. Meyer, J. E. Crow, P. P. Wise, and P. Schlottman, J. Appl. Phys. **69**, 5376 (1991).

[11] G. Wortmann and I. Felner, Solid State Commun. **75**, 981 (1990).

[12] M. Guillaume, P. Fischer, B. Roessli, A. Podlesnyak, J. Schefer, and A. Furrer, J. Appl. Phys. **75**, 6331 (1994).

[13] N. Rosov, J. W. Lynn, G. Cao, J. W. O'Reilly, P. Pernambuco-Wise, and J. E. Crow, Physica C **204**, 171 (1992).

[14] J. M. Tarascon, P. Barboux, P. F. Miceli, L. H. Greene, G. W. Hull, M. Eibschutz, and S. A. Sunshine, Phys. Rev. B **37**, 7458 (1988); E. Brecht, W. W. Schmahl, H. Fuess, H. Casalta, P. Schleger, B. Lebech, N. H. Andersen, and Th. Wolf, *ibid*. **52**, 9601 (1995).

[15] Chen Changkang, A. T. Boothroyd, Hu Yongle, F. R. Wondre, B. M. Wanklyn, and J. W. Hodby, Physica C **214**, 231 (1993).

[16] H.-D Jorstarndt, U. Walter, J. Harnischmacher, J. Kalenborn, A. Severing, and E. Holland-Moritz, Phys. Rev. B **46**, 14 872 (1992).

[17] M. E. López-Morales, D. Ríos-Jara, J. Tagüeña, R. Esudero, S. La Placa, A. Bezinge, V. Y. Lee, E. M. Engler, and P. M. Grant, Phys. Rev. B **41**, 6655 (1990).

[18] C. L. Lowe-Ma and T. A. Vanderah, Physica C **201**, 233 (1992).

[19] M. P. Nutley, Ph.D. thesis, University of Warwick, 1994; M. P. Nutley, A. T. Boothroyd, and G. J. McIntyre, J. Magn. Magn. Mater. **104–107**, 623 (1992).

[20] R. J. Weiss and A. J. Freeman, J. Phys. Chem. Solids **10**, 147 (1959).

[21] P. J. Brown, in *International Tables for X-Ray Crystallography*, edited by A. J. C. Wilson (Kluwer Academic, Dordrecht, 1992), Vol. C.

[22] S. Shamato, M. Sato, J. M. Tranquada, B. J. Sternlieb, and G. Shirane, Phys. Rev. B **48**, 13 817 (1993).

[23] H. Kadowaki, M. Nisha, Y. Yamada, H. Takeya, H. Takei, S. M. Shapiro, and G. Shirane, Phys. Rev. B **37**, 7932 (1988).

[24] J. W. Lynn, W.-H. Li, H. A. Mook, B. C. Sales, and Z. Fisk, Phys. Rev. Lett. **60**, 2781 (1988).

[25] See, for example, the comment of T. W. Clinton and J. W. Lynn, Physica C **174**, 487 (1991); and reply of H. Maletta, T. Chattopadhyay, and P. J. Brown, *ibid*. **174**, 489 (1991).

[26] J. A. Hodges, G. le Bras, P. Bonville, P. Imbert, and G. Jéhanno, Physica C **218**, 283 (1993).

[27] See, for example, T. Chattopadhyay, P. J. Brown, B. C. Sales, L. A. Boatner, H. A. Mook, and H. Maletta, Phys. Rev. B **40**, 2624 (1989); H. Maletta, E. Porschke, T. Chattopadhyay, and P. J. Brown, Physica C **166**, 9 (1990); J. W. Lynn, T. W. Clinton, W.-H. Li, R. W. Erwin, J. Z. Liu, K. Vandervoort, and R. N. Shelton, Phys. Rev. Lett. **63**, 2606 (1989).

[28] W.-H. Li, K. J. Chang, W. T. Hsieh, K. C. Lee, J. W. Lynn, and H. D. Yang, Phys. Rev. B **48**, 519 (1993).
[29] H. D. Yang, M. W. Lin, C. K. Chiou, and W. H. Lee, Phys. Rev. B **46**, 1176 (1992).
[30] H. Lutgemeier, J. Magn. Magn. Mater. **90**, 633 (1990).
[31] S. D. Goren, C. Korn, H. Riesemeier, and K. Luders, Phys. Rev. B **47**, 2821 (1993).
[32] H. Casalta, P. Schleger, E. Brecht, W. Montfrooij, N. H. Andersen, B. Lebech, W. W. Schmahl, H. Fuess, R. Liang, W. N. Hardy, and T. Wolf, Phys. Rev. B **50**, 9688 (1994).
[33] B. Lebech and M. Nielsen (unpublished).
[34] R. A. Cowley and S. Bates, J. Phys. C **21**, 4113 (1988).
[35] M. J. Cooper and R. Nathans, Acta Crystallogr. **23**, 357 (1967).